Molecular Neurobiology (2024) 61:3724–3741
https://doi.org/10.1007/s12035-023-03733-w

Restoring Synaptic Function: How Intranasal Delivery of 3D-Cultured hUSSC Exosomes Improve Learning and Memory Deficits in Alzheimer's Disease

Masoumeh Pourhadi[1] · Hakimeh Zali[1,2] · Rasoul Ghasemi[3] · Mehrdad Faizi[4] · Faraz Mojab[5] · Mina Soufi Zomorrod[6]

Received: 29 April 2023 / Accepted: 20 October 2023 / Published online: 27 November 2023

Abstract

Memory problems are often the first signs of cognitive impairment related to Alzheimer's disease (AD), and stem cells and stem cell-derived exosomes (EXOs) have been studied for their therapeutic potential to improve the disease signs. While many studies have shown the anti-inflammatory and immunomodulatory effects of stem cells and exosomes on improving memory in different AD models, there is still insufficient data to determine how they modulate neural plasticity to enhance spatial memory and learning ability. Therefore, we conducted a study to investigate the effects of exosomes derived from 3D-cultured human Unrestricted Somatic Stem Cells (hUSSCs) on spatial memory and neuroplasticity markers in a sporadic rat model of AD. Using male Wistar rats induced by intracerebral ventricle injection of streptozotocin, we demonstrated that intranasal administration of hUSSC-derived exosomes could decrease Aβ accumulation and improve learning and memory in the Morris water maze test. We also observed an increase in the expression of pre-synaptic and post-synaptic molecules involved in neuronal plasticity, including NMDAR1, integrin β1, synaptophysin, pPKCα, and GAP-43, in the hippocampus. Our findings suggest that intranasal administration of exosomes can ameliorate spatial learning and memory deficits in rats, at least in part, by increasing the expression of neuroplasticity proteins. These results may encourage researchers to further investigate the molecular pathways involved in memory improvement after stem cell and exosome therapy, with the goal of increasing the efficacy and safety of exosome-based treatments for AD.

Keywords Alzheimer's disease · 3D-Cultured human Unrestricted Somatic Stem Cell · Exosomes · Learning and memory deficits · Neuroplasticity · NMDAR1 · GAP-43 · pPKCα · Synaptophysin · Integrin β1

Introduction

Alzheimer's disease (AD) is the most prevalent neurodegenerative disease and is considered the main cause of dementia in the world [1, 2]. The pathophysiology of AD is complex, but the main causes, including the abnormal activity of mitochondria, blood vessels, ion channels, and dysfunctional synapses, are believed to lead to neuronal damage [3]. For healthy brain function, the proper activation and inhibition state of the synapses are significantly pivotal. Therefore, changes in neuronal or synapse activity/inhibition are linked to the progression of AD. The changes in beta-amyloid (Aβ)

✉ Hakimeh Zali
h.zali@sbmu.ac.ir

✉ Rasoul Ghasemi
rghasemi60@gmail.com

[1] Department of Tissue Engineering and Applied Cell Sciences, School of Advanced Technologies in Medicine, Shahid Beheshti University of Medical Sciences, Tehran, Iran

[2] Medical Nanotechnology and Tissue Engineering Research Center, Shahid Beheshti University of Medical Sciences, Tehran, Iran

[3] Department of Physiology, School of Medicine, Shahid Beheshti University of Medical Sciences, Tehran, Iran

[4] Department of Pharmacology and Toxicology, School of Pharmacy, Shahid Beheshti University of Medical Sciences, Tehran, Iran

[5] Department of Pharmacognosy, School of Pharmacy, Shahid Beheshti University of Medical Sciences, Tehran, Iran

[6] Department of Hematology and Cell Therapy, Faculty of Medical Sciences, Tarbiat Modares University, Tehran, Iran

homeostasis may lead to neuronal dysfunction and decreased levels of synaptophysin and the number of synapses in the brain [4, 5].

Glutamate is a crucial excitatory neurotransmitter with essential roles in mammalian memory and synaptic plasticity [6]. N-methyl-d-aspartate (NMDA) is a type of glutamate receptor (ion channel) involved in fast excitatory neurotransmission. It has been proven that Aβ oligomers can be toxic to NMDA receptors and play a key role in cognition dysfunctionality [7]. Excessive glutamate release (excitotoxicity) has been implicated in neuronal cell death through glutamate receptors such as NMDARs, and this condition can be induced by Aβ or decreased glutamate uptake [8].

The growth-associated protein 43 (GAP-43) contains various parts, such as binding to the membrane domain, calmodulin domain, and protein kinase C domain [9]. In synapses, GAP-43 has a regulating role in axonal growth, function of pre-synapse vesicle, and neuronal plasticity via being a substrate for protein kinase C (PKC) [10–12]. Its expression changes in neuronal damage (axonal outgrowth) and presynaptic rearrangement (memory formation and development). In addition, studies showed that its phosphorylation process via PKC activity is decreased in AD [13].

Stem cells and their secretions regulate neurons and promote neuro-regeneration. Hence, they may play the significant role in neuronal circuit remodeling and also in learning processes and memory formation [14–25]. New therapies in neurodegenerative disease, such as the administration of stem cells and stem cell-derived products, require an easily accessible source [26]. Human Unrestricted Somatic Stem Cells (hUSSCs) can be an appropriate source for the new therapies due to the absence of ethical issues for hUSSC extraction and the considerable capacities [27]. One of the most important characteristics of hUSSCs is their secretions, which contains various factors involved in tissue growth, differentiation, division, and repair. Compared to other stem cells, hUSSCs have lower expression of MHC-II molecules, and they can be expanded under good manufacturing practice (GMP) standards. USSCs have shown great promise in various research and therapeutic applications due to their regenerative potential and immunomodulatory properties. They hold significant potential in tissue engineering, regenerative medicine, and treating various medical conditions. Moreover, the use of hUSSCs in research and clinical settings benefits from the fact that they can be obtained from umbilical cord blood, which is a readily available source with ethical advantages. This makes hUSSCs an attractive option for stem cell-based therapies and experimental studies, opening up new possibilities in the field of regenerative medicine [27, 28]. In addition, the therapeutic effects of 3D-cultured MSCs derived EXOs on AD improvement have been examined in a few studies. As the biological and cellular responses in 2D and 3D cell cultures differ significantly [29], in this study, hUSSCs were cultured in 3D conditions by the liquid overlay technique (LOT), and the medium was collected for exosome extraction. LOT is a scaffold-free technique with easy operation and an affordable cost. Although various methods have been applied to form spheroids (based on scaffold or scaffold-free), LOT is the most investigated technique [30–33]. Then, the protective effects of EXOs were investigated in the C6 cell model induced by L-glutamate and AD rat models induced by streptozotocin (STZ) to detect improvements in cell viability, cognitive function, spatial learning, and memory. As STZ decreases the neural plasticity markers' levels, we investigated whether EXOs can change the neuroplasticity markers' expression in the hippocampus.

Methods

Study Design

This study involves both in vitro and in vivo experiments to investigate the effects of exosomes derived from human umbilical cord blood-derived mesenchymal stem cells (hUSSCs) on C6 cells and in a rat model of Alzheimer's disease (AD). In the in vitro section, hUSSCs were cultured by the LOT technique to form spheres, and the conditioned medium was collected to extract EXOs. The neuroprotective effects of EXOs were studied on 2D and 3D-cultured C6 cells in oxidative condition (L-glutamate induced neurotoxicity) by flow cytometry, MTT test, and AO/PI staining. In the in vivo section, the effects of EXOs were investigated in the STZ-AD rat model. After 2 weeks of intranasal administration of treatments (five times), the Morris water maze (MWM) test was conducted to evaluate the STZ and EXOs effects on different criteria in different groups. The neural plasticity markers were assessed by western blot and IHC (Fig. 1).

hUSSCs Isolation and Culture

Human umbilical cord blood was extracted with written consent from the mothers, in accordance with the ethics and safety committees of Tarbiat Modarres University and Gandi Hospital (Tehran, Iran). To lysis red blood cells, ammonium chloride (NH4Cl) (Sigma, Germany) was used, and Ficoll-Hypaque (Sigma, Germany) was added to the cell solution. The Ficoll-Hypaque and cell solution were then centrifuged at 400 g for 30 min at room temperature. After extraction of the mononuclear cell layer, it was diluted with Hank's balanced salt solution (HBSS) and centrifuged at 400 g for 10 min. The cells were then washed with PBS and seeded onto 75 cm^2 tissue-culture flasks (SPL, Korea) in DMEM/F12 + 20% fetal bovine serum (FBS), 2 mM glutamine, 100 mg/ml streptomycin, and 100 U/ml penicillin (Biocera,

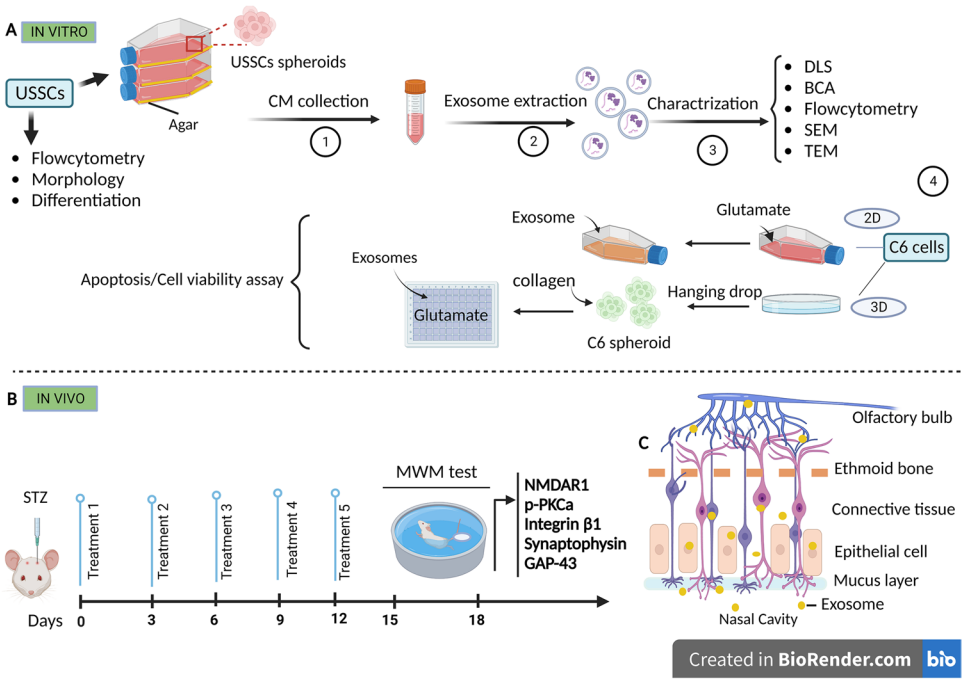

Fig. 1 The workflow of studying the effects of intranasal administration of EXOs on the AD rat model. **A** In vitro. **B** In vivo. **C** The path of exosome transfer after intranasal administration. The figure created with BioRender.com

France). The cells were maintained in a humidified incubator at 37 ℃ and 5% CO_2.

hUSSCs Characterization

To evaluate the immuno-phenotypic properties of hUSSCs, cell surface markers were analyzed in the third passage. To achieve this, hUSSCs were collected using 0.25% trypsin–EDTA and modified to 1×10^6 cells/mL. Mesenchymal stem cells were labeled with CD34-PE, CD45-FITC, CD44-PE, CD13-FITC, and CD90-APC antibodies and were incubated in the dark for 30 min. After incubation, cells were centrifuged at 300 g for 5 min, and specific fluorescence was detected using BD FACS Calibur. The resulting data were analyzed with FlowJo software.

To differentiate hUSSCs into adipogenic and osteogenic lineages, 1×10^5 cells from the third passage were placed in a 6-well plate and allowed to reach a confluency of 80–90% for several days. Differentiation was induced by replacing the previous medium with a differentiating medium containing dexamethasone, indomethacin, and IBMX (isobutyl-methylxanthine) for adipogenic induction, and ascorbic acid, beta glycerophosphate, dexamethasone, and 10% fetal bovine serum with low glucose DMEM medium for osteogenic induction. The medium was changed every 2–3 days for 21 days, and DMEM/F12 was used as a control.

Intracellular lipid vacuoles were examined by staining the cells with Oil Red O. The cells were washed with PBS, fixed with 4% paraformaldehyde for 45 min and then treated with Oil Red O dye for 30 min at 37 °C. The stained areas were visualized using an inverted microscope. Mineralization and calcification nodules were investigated by staining the cells with Alizarin. The cells were washed and fixed with 4% paraformaldehyde for 45 min and then stained with 2% alizarin with a pH range of 2.4–4.4 for 30 min at 37 °C. The stained areas were also visualized using an inverted microscope.

Optimizing hUSSCs Cell Number for 3D Spheroids Formation by Liquid Overlay Technique (LOT)

In order to optimize the number of hUSSCs for 3D spheroid formation by the liquid overlay technique (LOT), 25-cm^2 flasks were used and covered with 4% agar. The culture medium was added to a maximum volume of 12 ml. Different numbers of stem cells from the 3rd passage were added to the flasks to determine the appropriate number for spheroid formation without requiring medium changes. The cell numbers tested included 1250, 2500, 5000, 10000, 20000 and 40000 for every 100 µl of culture medium. The cells were then cultured on agar and incubated for 5 days. After 5 days, the spheroids were examined for formation, number, size, and the survival rate of cells; besides, the medium color changes. The spheroids were washed with PBS and stained with AO/PI dye (Nexcelom bioscience) and examined under fluorescent microscopes to determine the live cell percentage. Spheroid sizes and numbers were checked with a light microscope.

Exosome Extraction and Characterization

hUSSCs spheroids from the passage 3–4 were cultured in FBS-free medium for 48 h, and then the conditioned medium

was collected and centrifuged at 2500 rpm for 15 min and at 4000 rpm for 20 min to remove cellular debris. The remaining medium was then passed through a 0.45 µm filter to extract the exosomes using an extraction kit (EXOCib kit, Iran). The concentration of the exosomes was determined using a bicinchoninic acid (BCA) kit (Bio Idea Iran, Tehran), and their specific markers (CD9, CD63, and CD81) were detected using flow cytometry. To visualize the exosomes, they were incubated on a grid for 15 min and then treated with a solution containing glutaraldehyde, paraformaldehyde, tannic acid, and PBS for 10 min. The grid was then imaged using a transmission electron microscope (TEM) (FEI, USA). The size of the exosomes was measured using dynamic light scattering (DLS) (Malvern Instruments, Malvern, UK). Finally, the exosomes were incubated with 3% glutaraldehyde, washed with PO4 buffer, and imaged using a scanning electron microscope (Tecnai SEM).

2D and 3D-C6 cells Treatment with EXOs in L-glutamate Toxic Condition

To study the effects of EXOs in pre-treatment and post-treatment experiments in 2D condition, 5×10^4 C6 cells were seeded in 6 well plates, and 10 mM L-glutamate was added [34]. After 24 h, the medium was completely removed, and 0.7 and 7 µg/ml EXO were used in the groups and incubated for 24 h. For the pre-treatment study, 0.7 and 7 µg/ml EXO were added, and cells were incubated for 24 h; then, the medium was completely removed, and 10 mM glutamic acid was added for 24 h. The MTT assay was used for C6 cell viability calculation. Moreover, the samples were collected for apoptosis analysis by flow cytometry.

For 3D condition, C6 cells suspension was counted, and 20 µl droplets containing 10,000 cells were placed on the lid of the petri dish and then placed in the incubator. After 48 h, it was washed with the culture medium, and the spheroids were collected and centrifuged at 4000 rpm for 10 min. The spheroids were transferred to agar-coated flasks and incubated for 48 h. After incubation, the spheroids were collected and centrifuged at 4000 rpm for 10 min. The precipitated spheroids were mixed with 2.5% collagen to simulate the extracellular matrix. To prepare it, collagen, water, phenol red, and NaOH 5Normal were needed. After mixing all the items in the microtube on ice, spheroids were added to the mixture and seeded into a 96-well plate with 100 µl medium for 24 h. Then, they were treated with a 10 mM concentration of L-glutamate. Treatment with EXOs was performed at a concentration of 0.7 and 7 µg/ml 24 h after glutamate exposure for 3 days, in the post-treated group. In the pre-treated groups, cells were treated with EXOs for 3 days, and then L-glutamate was added. The spheroids were collected and washed with PBS and then incubated with 20 µl of AO/PI for 30 min, and the live and dead cells were examined under a fluorescent microscope.

Animals

Adult male Wistar rats (250–300 g) were purchased and divided into the standard cages with available food and water on a 12 h dark/12 h light cycle. The room temperature and humidity were controlled (23–27 °C and 50–60%). Minimizing pain and also the number of animals used in the study were considered. All in vivo experiments were approved by the ethics committee of Shahid Beheshti University of Medical Sciences (approval code: IR.SBMU.AEC.1401.005) and followed the NIH Guide for animal use.

AD Model Induction and Exosome Administration

Streptozotocin (STZ) was purchased from Sigma-Aldrich (St. Louis, MO, USA) and was dissolved freshly in normal saline. On surgery day, the rats ($n = 8$–10 per group) were anesthetized with an IP injection of xylazine (10 mg/kg) and ketamine (100 mg/kg). The rats were fixed inside a stereotaxic device, and by following the Paxinos brain atlas, STZ or normal saline was injected directly into the intracerebral ventricle (ICV) using a 10 µl Hamilton syringe (gauge 30) with the polyethylene tube (AP − 0.8, ML 1.5, DV − 3.5). STZ (3 mg/kg) or the vehicle was administered at a rate of 1 µl/min [35]. The rats were randomly and equally divided into six groups as follows: (1) Sham/vehicle group, normal control rats underwent surgery and received 7–10 µl of saline on surgery day and 10 µl of PBS in every nostril on treatment days (five-time treatment in 2 weeks); (2) STZ group, rats received 7–10 µl of STZ on surgery day, and 10 µl PBS in every nostril on treatment days; (3) STZ + EXO 0.7 group, on treatment days, STZ-injected rats received 10 µl of 0.7 µg/mL EXO in every nostril; (4) STZ + EXO 7 group, on treatment days, STZ-injected rats received 10 µl of 7µg/mL EXOs in every nostril; (5) STZ + EXO 70 group, on treatment days, STZ-injected rats received 10 µl of 70 µg/mL EXO in every nostril; and (6) normal saline + EXO group, normal control rats received 7–10 µl of saline on surgery day and 10 µl of 70 µg/mL EXOs in every nostril on treatment days. Rats were continuously treated with 3D-Exo solution or PBS. EXOs were resuspended in a sterile PBS solution at different concentrations. For intranasal administration, rats were anesthetized with ketamine before being carefully intranasally administered with PBS solution or EXOs at a rate of 2 µl/min. Overall, each rat received 100 µL of vehicle or EXOs in the treatment procedure.

Morris Water Maze Test

MWM is a behavioral test to investigate the effects of treatments on spatial learning and memory abilities in rats [35, 36]. Prior to the experiment, the rats were placed in a darkened test room for approximately 1 h. On three consecutive days of training, each rat was evaluated in four trials. At the start of each experiment, the rat was placed in the water facing the wall of the maze and given 90 s to swim and find the platform. Additionally, on the first day, at the beginning of the experiment, each rat was given 20 s to habituate to the platform. After each trial, the rat remained on the platform for 20 s (the platform was either discovered by the rat or manually directed onto it). On the day of training, each trial was started from a randomly chosen position. On the fourth day, the platform was removed from the water tank, and rats were allowed to swim for 60 s after being placed in the opposite quadrant (opposite to the target quadrant). The visible platform test was then performed to evaluate sensory and motor abilities by performing four trials similar to training days, while the platform was covered with aluminum foil and located above the water level in the target opposite quadrant. The recorded videos on the training days and probe day of each rat were processed by a computerized system (Noldus EthoVision, 11.1 versions) to find the escape latency and distance swam to reach the platform on training days and time spent in the target quadrant, time spent on the platform, platform crossing frequency, the latency to the first cross of the platform, and speed on probe day.

Tissue Preparation

On the last day of the behavioral tests (18 days), for the IHC study, each rat was anesthetized by using ketamine and xylazine. Rats were perfused transcardially with 0.1 M PBS followed by neutral-buffered formalin (10%). The whole brains were extracted and maintained in formalin for at least 48 h. Then, the tissue processor was used to prepare the tissue samples and then embedded in paraffin blocks. Additionally, after deep inhalation of CO2, animals were sacrificed by cervical dislocation, and hippocampi were removed and transferred to – 196 °C; then, all samples were stored at – 80 °C until western blot analysis.

Congo Red Staining

For preliminary histopathological examination, tissue sections with 5 µm thickness were stained with Congo red (Shimi Pajhouhesh Asia, Iran) to reveal amyloid plaque deposition in the hippocampal regions. The Aβ plaque load was quantitatively assessed using Congo red staining. For this evaluation, 10 random areas of the hippocampus were microscopically selected, and the percentage of area occupied by Aβ was assessed. The data were then statistically evaluated.

Immunofluorescence Staining

The sections (triplicate per marker per group) were placed in the TBS 1X solution (Sigma-T5912) and subjected to antigen retrieval in a microwave. The slides were washed with PBS (Sigma-P4417), and then Triton 0.3% was added for 30 min to permeabilize the cell membrane. The samples were washed with PBS, and then 10% goat serum was added to the samples and incubated for 45 min at 37 °C to block the secondary antibody reaction. The slides were incubated with primary antibodies: GAP43 (1:100, orb256550 Biorbyt, Cambridge, UK), synaptophysin (1:100, orb214639, Biorbyt, Cambridge, UK), and integrin β1 (1:100, orb251610, Biorbyt, Cambridge, UK) diluted with PBS at 4 °C for 24 h. The sections were then incubated with a goat Anti-Rabbit IgG (H + L) secondary antibody (FITC) (1:150, orb688925, Biorbyt, Cambridge, UK). The slides were placed in a 37-degree incubator (AriaTeb model) for 90 min. Then, the sections were incubated with DAPI (1:1000, Sigma-Aldrich, D9542 St. Louis, MO, USA) for 20 min, and images were taken using a florescent Olympus microscope.

Western Blot

Hippocampal tissues were lysed using RIPA and protease inhibitor buffer for 1 h at 4 °C; then, the samples were centrifuged at 13000 rpm for 20 min. To determination of protein concentration, 5 µl of supernatant was boiled with 5 µl of NaOH in a water bath. Next, 50 µl of mixed buffer were added and incubated at room temperature for 10 min (mixed buffer: NA2CO3, CUS04.5H2O, and sodium potassium tartrate all in distilled water were prepared in the proportions of 100 µ*l*, 1 µ*l*, and 1 µ*l*). Samples were transferred to a plate and Folin was added to samples and incubated in the dark room for 30 min. The absorption of samples was read by a Biotek device (ELISA Reader) at a wavelength of 630 nm.

Protein extracts (10–20 µg) were separated by electrophoresis on a 10–12% sodium dodecyl sulfate–polyacrylamide gel ($n = 3$ per group). The blots were transferred to a nitrocellulose membrane at 4 °C, and the blocker buffer was added to block nonspecific binding sites. They were then incubated with primary antibodies, including monoclonal mouse anti-p-PKC α Antibody (sc-377565, 1:1000, Santa Cruz Biotechnology, CiteAb, UK), polyclonal rabbit anti-NMDAR1 (GTX133097, 1:1000, GeneTex, USA), and polyclonal rabbit anti-GAPDH (GTX100118, 1:1000, GeneTex, USA) overnight at 4 °C, followed by secondary antibodies incubation, goat anti-Rabbit IgG, and sc-516102 m-IgGκ BP-HRP, (1:1000, Santa Cruz Biotechnology, CiteAb, UK) for 2 h at room temperature. Immunoreactive proteins were

detected using a chemiluminescent substrate (Pierce ECL Western Blotting Substrate, Perkin Elmer), and the results were analyzed by Image J.

Statistical Analysis

Data were analyzed using GraphPad Prism 7.01 software. One-way or two-way ANOVA was used according to the experimental design. Appropriate post hoc tests were performed in the presence of significant treatment effect (one-way ANOVA) or significant interaction between the STZ model and treatment (two-way ANOVA). Student's *t*-test was used to compare two experimental groups when appropriate. A P-value < 0.05 was considered significant. A sample size of 8–10 rats/group was selected based on our wide previous experience.

Results

hUSSCs Flowcytometry Analysis and Differentiation Potential

We examined hUSSCs for the differentiation capacity and phenotypic markers. hUSSCs appeared spindle-shaped and adhered to the bottom of the culture flask (Fig. 2A). Flow cytometry analysis showed the positive markers as follows: CD44 97.7%, CD90 99.8%, CD13 4.7%, CD34 0.36%, and CD45 0.42% (Fig. 2B). Lipid vacuoles (rich in triglycerides) were stained by Oil Red O in hUSSCs cultured in the adipogenic inducing medium after 21 days. Mineral deposits were evident in hUSSCs cultured for 21 days in an osteogenic differentiation medium but not in control hUSSCs. Alizarin Red staining was performed to assess the mineralization (Fig. 2C). These results indicate that the hUSSCs can be differentiated into adipocytes and osteocytes.

Adjusting hUSSCs Number for LOT 3D Culture

The different hUSSC numbers, including 1250, 2500, 5000, 10000, 20,000, and 40000 cells/100 µl medium, were cultured by the LOT technique. After 5 days, the spheroids were stained with AO/PI to detect whether the cells were alive or not (Figs. 3A and B). AO/PI staining shows that the color change was noticeable and significant in the last group. The survived hUSSC cells percent were 87.32 ± 0.82, 87.45 ± 1.3, 84.7 ± 1.86, 80.42 ± 4.58, 83.77 ± 2.58, and 63.49 ± 3.71, respectively (Fig. 3C). The number of spheres in the groups was counted, and the average in every group was 7.6 ± 1.83, 14.5 ± 2.53, 8.6 ± 0.92, 12.8 ± 4.53, 26.33 ± 3.73, and 11.32 ± 2.67, respectively (Fig. 3D). The average sphere diameter in different groups was 0.63 ± 0.01, 0.69 ± 0.01, 1.32 ± 0.16, 1.7 ± 0.38, 2.35 ± 0.21, and 0.8 ± 0.24 mm,

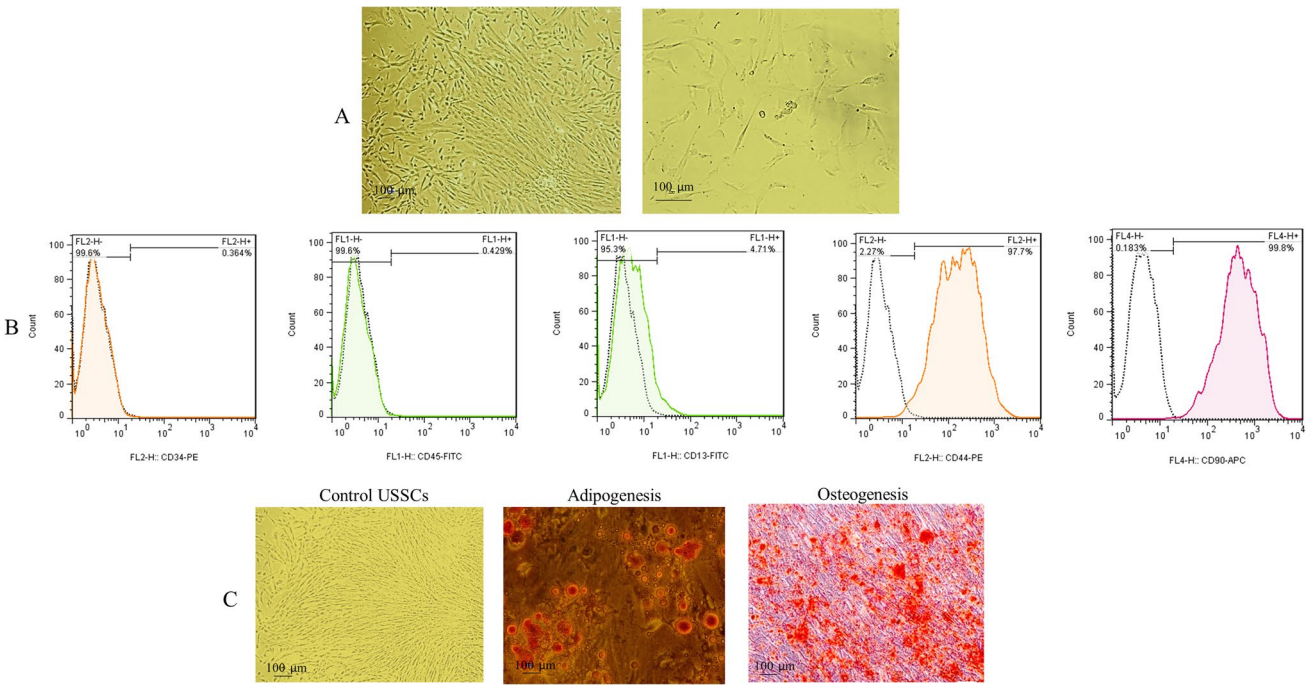

Fig. 2 Human Unrestricted Somatic Stem Cell (hUSSC) characterization. **A** Inverted light microscope shows hUSSCs with a spindle-like shape that demonstrates the morphological characteristics of MSCs. Scale bar: 100 μm. **B** Flow cytometry analysis of human hUSSCs for CD 13, CD 90, CD 44, CD 34, and CD 45. **C** hUSSC adipogenic and osteogenic differentiation. The differentiated cells have been stained with Oil Red O and Alizarin Red, respectively

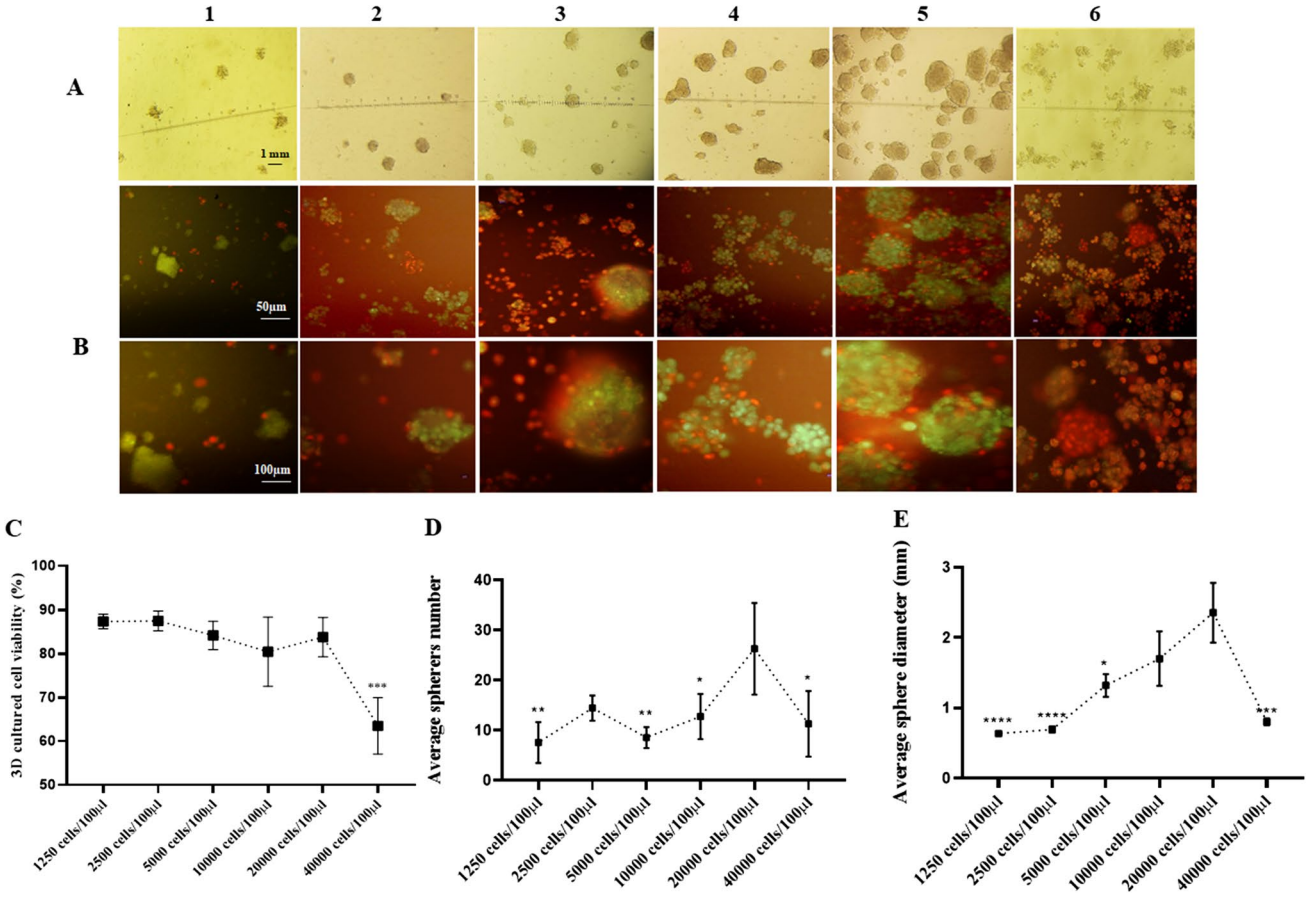

Fig. 3 **A** hUSSCs spheroid 5 days after culturing on 4% agar for finding the appropriate cell number for LOT in 25 cm^2 flasks under the light microscope. **B** AO/PI fluorescent staining for determining the presence of live and dead cells in spheroids. (1) Cell culture medium containing 1250 hUSSCs/100 µl. (2) Cell culture medium containing 2500 stem cells/100 µl. (3) Cell culture medium containing 5000 stem cells/100 µl. (4) Cell culture medium containing 10,000 stem cells/100 µl. (5) Cell culture medium containing 20,000 stem cells/100 µl. (6) Cell culture medium containing 40,000 stem cells/100 µl. Scale bars: 0.1 mm, 50 µm, and 100 µm. **C** Cell viability of hUSSCs in spheroid culture. **D** Average sphere numbers in different groups. **E**) Average sphere diameter (mm). The data is presented as mean ± SD. $*P<0.05$, $***P<0.001$, and $****P<0.0001$ compared to 20,000 cell/100 µl

respectively (Fig. 3E). In all groups except 20000 cells/100 µl, the spheroids were not stable, and most of the cells did not participate in spheroid formation; hence, they were stained in red color after 5 days. We chose 20000 cells/100 µl as the optimum number of hUSSCs for 3D culture with LOT in 25-cm2 flasks in our study.

Exosome Characterization: Flowcytometry, Size, Concentration, and Morphology

EXOs were extracted by the EXOCib kit and characterized by different tests. Flow cytometry analysis showed that the positivity of selected markers was as follows: CD81: 72.5, CD63: 73.9% and CD9: 75.8% (Fig. 4A). The size of EXO was analyzed using DLS, and the average diameter for EXO was 45–100 nm (Fig. 4B). The concentration of EXO was 9507.1 mg/ml. The morphology and size of isolated EXO was analyzed using SEM and TEM. The SEM visualization showed that the EXO size ranged from 35 to 130 nm (Fig. 4C). TEM analysis showed the characteristic spheroid shape in EXO (Fig. 4D).

Exosomes Improve Cell Viability in L-glutamate-Induced Cytotoxicity

C6 cells were pre-treated and post-treated with different concentrations of EXOs in glutamate-induced cytotoxic conditions. The MTT assay was conducted in different groups 24 h after the last treatment (Fig. 5A). The EXO-treated groups had increased cell viability. Every group's result was normalized to the glutamate and the control group. The flow cytometry test was conducted to find apoptotic and live cell percentages. The flow cytometry results showed that Exo increases cell viability in toxic conditions. The live cell percentage in the glutamate group was 66.4% improved in the EXOs groups (85.4–90.1%), and the necrotic cell percentage in the glutamate group was 11.7% which was improved in

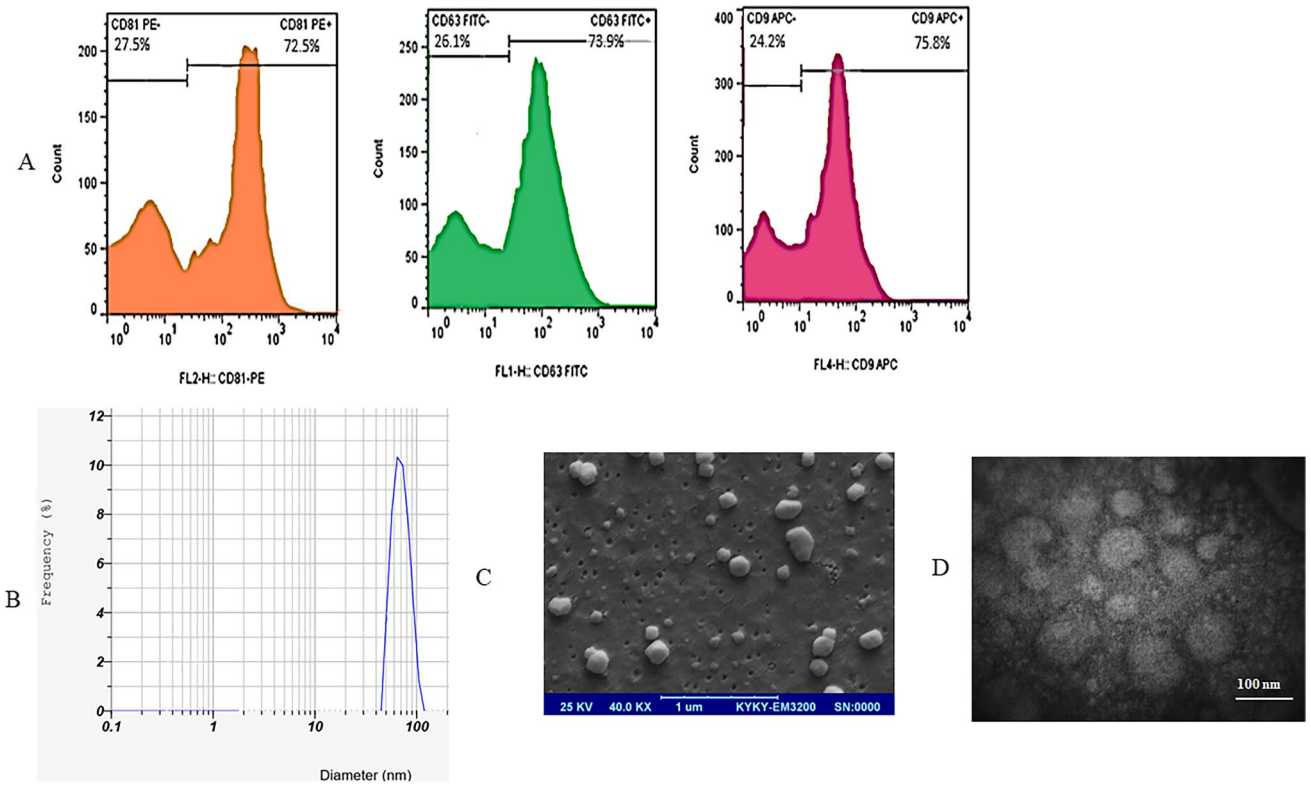

Fig. 4 Flow cytometry, DLS, SEM, and TEM analysis of EXO. **A** Flow cytometry showed three positive markers for exosomes: CD81, CD63 and CD9. **B** Particle size distribution measured by DLS. **C** Morphology of Exo observed by SEM. **D** Morphology of Exo observed by TEM

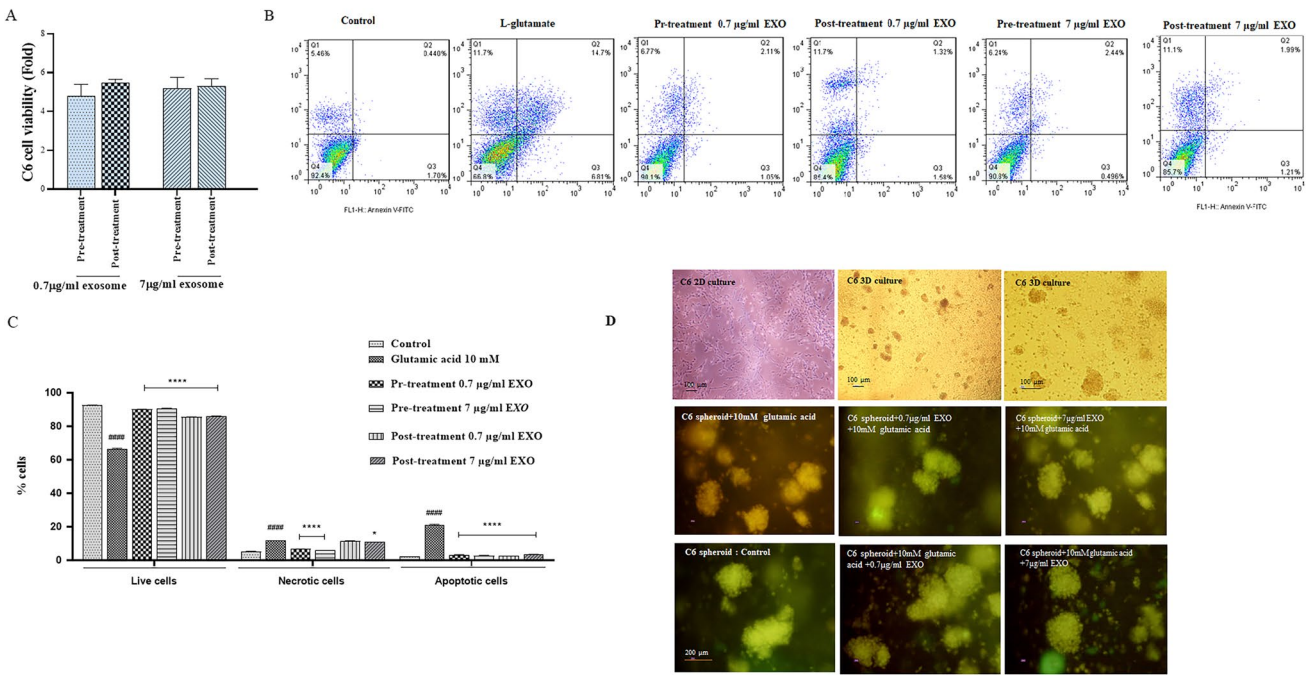

Fig. 5 **A** 2D-C6 cell viability in oxidative condition (10 mM L-glutamate) after pre-and post-treatment with EXO (MTT results). **B**, **C** Flow cytometry data showing the live and apoptotic C6 cell percent. The data is presented as mean ± SD. $^{****}P < 0.0001$ compared to glutamate group. $^{\#\#\#\#}P < 0.0001$ compared to control group. **D** AO/PI dye for staining C6 live and dead cells in 3D-collagen-based condition after pre-treatment and post-treatment with EXO

the treated groups (6.24–11.7%). In the glutamate group, the percentage of apoptotic cells was 21%, which was improved by EXO to 2.3–3.5% (Figs. 5B and C).

To analyze EXOs effects on C6 cell viability in 3D culture conditions, spheroids were cultured in collagen to simulate the extracellular matrix. Spheroids were treated with Exo likewise in the previous section, and after 24 h, spheroids were stained with AO/PI and were examined with a fluorescence microscope. All images showed improved cell viability when compared to the L-glutamate group (Fig. 5D).

EXO Improve Learning and Memory Deficiencies in Sporadic AD Rats

The MWM test is a reliable way to measure spatial memory and learning. Figure 6 shows that after 3 days of training in the STZ-EXO groups, the learning patterns of rats improved. There was a statistically significant difference in the mean escape latency between the groups using the two-way ANOVA repeated measures analysis ($F(6, 147) = 17.12$, $P < 0.0001$). According to the Tukey's post hoc test, STZ-treated animals have significantly longer escape latencies than the control group on all three training days (days 1 and 3 ($p = 0.01$) and day 2 ($p = 0.0001$)) (Fig. 6A). This data confirms STZ-related learning deficit. The STZ-induced escape latency time was reduced dose-dependently by EXO treatments. In comparison to the STZ group: (1) EXO 0.7-treated animals did not have a significant difference in escape latency times on all 3 days (day 1 ($p = 0.9476$), day 2 ($p = 0.8594$), and day 3 ($p = 0.9145$)); (2) EXO 7-treated group animals had lower escape latency on days 1 ($p = 0.0163$), 2 ($p = 0.0244$), and 3 ($p = 0.3406$); and (3) Exo

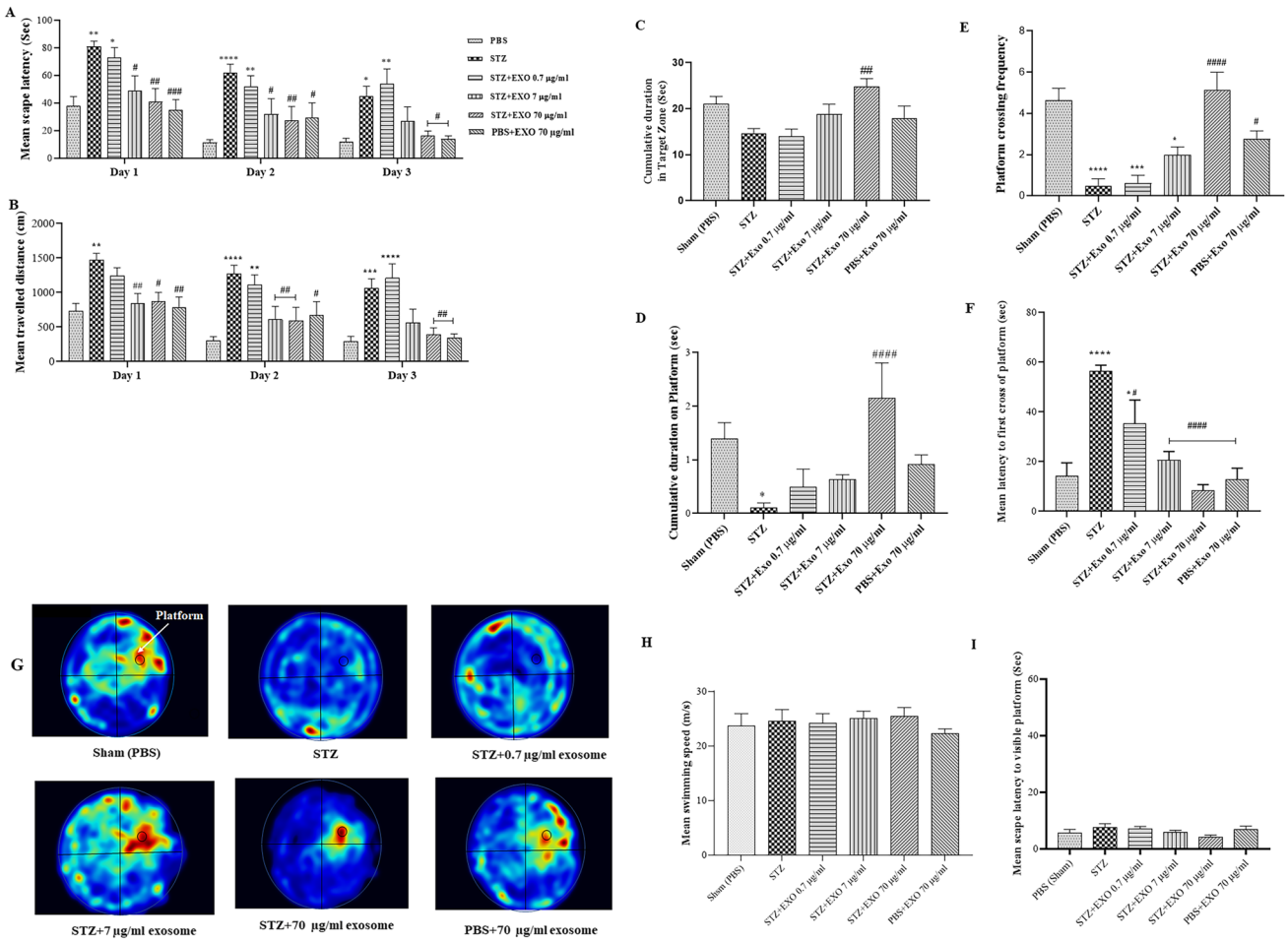

Fig. 6 The effect of STZ, EXO (0.7, 7, and 70 µg/ml), and PBS administration on spatial learning capability during training days and probe day. **A** The mean escape latency to find the hidden platform. **B** The mean traveled distance to reach the platform. **C** The time spent in the target area. **D** The time spent on the platform. **E** The platform crossing frequency. **F**, The mean latency to the first cross of the platform in the probe test. **G** Mean heatmap visualization of animal performance. The figures are the merged results in every group ($n = 8$–10). **H** Mean swimming velocity on prob day. **I** Mean scape latency to the visible platform on prob day. All values are represented as mean ± SEM ($n = 8$–10). $^{*}p < 0.05$, $^{**}p < 0.01$, $^{***}p < 0.001$, and $^{****}p < 0.0001$ versus control (Sham). $^{\#}p < 0.05$, $^{\#\#}p < 0.01$, $^{\#\#\#}p < 0.001$, and $^{\#\#\#\#}p < 0.0001$ versus STZ

70 treatment reduced escape latency (day 1 ($p = 0.0014$), day 2 ($p = 0.0068$), and day 3 ($p = 0.0357$)) on all 3 days. The two-way ANOVA repeated measures analysis showed a statistically significant difference between the groups for the mean traveled distance (F (6, 147) = 18.58, P 0.0001), as shown in Fig. 6B. In comparison to the control group, as determined by post hoc Tukey's test, the STZ-treated group had an increased mean traveled distance (day 1 ($p = 0.0011$), day 2 ($p = 0.0001$), and day 3 ($p = 0.0005$)).

In addition, the test showed that there was no significant difference between the STZ and STZ + EXO 0.7 group on day 1 ($p = 0.6827$), day 2 ($p = 0.9113$), and day 3 ($p = 0.9461$) in the mean traveled distance (Fig. 6B). Between the STZ and EXO 7 groups on day 1 and day 2, there was a significant decrease in mean traveled distance on day 1 ($p = 0.0078$), day 2 ($p = 0.0040$), and day 3 ($p = 0.0506$). The STZ + EXO 70 (day 1 ($p = 0.0110$), day 2 ($p = 0.0032$), and day 3 ($p = 0.0035$)) experienced significant decreases on all three days. These results suggest that the treatment with EXO was effective in reducing the distance swam to find the platform.

On day four, memory retention capacity was evaluated with a probe test. One-way ANOVA analysis of the time each group spent in the target quadrant revealed no statistically significant difference (F (6, 50) = 1.401, $P = 0.2329$), except for the EXO70 group ($P = 0.0083$) (Fig. 6C). Moreover, EXO 70-treated groups spent the most time on the platform position (F (6, 49) = 4.465, $P = 0.0011$). The post hoc test found that the EXO 70-treated group has increased mean spending time on the platform in comparison to the STZ group ($p = 0.0005$ and $p = 0.0158$, respectively) (Fig. 6D). The mean platform crossing frequencies of different groups were examined during the probe test. A dose-dependent significant difference between the groups was found by one-way ANOVA (F (6, 49) = 10.15, $P < 0.0001$) (Fig. 6E). Further analysis revealed that the STZ group was less likely to reach the platform location, and EXO 0.7 and 7 groups did not show a statistically significant difference from the STZ group ($p = 0.2903$ and 0.9998, respectively). However, compared to the STZ group, EXO70 was able to significantly increase the frequency of platform crossing ($p < 0.0001$ and $p = 0.0006$, respectively). The mean latency of the first platform crossing was assessed in groups, and as depicted in Fig. 6F, STZ and treated groups differed significantly (F (6, 49) = 11.77, $P < 0.0001$). STZ group animals needed more time to reach the platform, but treatment with EXO7 and EXO70 decreased the time ($p < 0.0001$). The heatmap visualization in Fig. 6G shows the performance of the animal on probe day. A black circle indicates the location of platform in each image. All the trials of each group have been superimposed onto these images. It shows that animals in the STZ and STZ + EXO 0.7 treated groups swim in the wrong zones, especially in the peripheral parts of the pool (thigmotaxis). On the other hand, in EXO70 group, they mainly swim in the target zone, and there is almost no thigmotactic behavior. On probe day, the swimming speeds of all animals were measured to determine whether STZ and/or EXOs affect motor function. There was no statistically significant difference between the groups using one-way ANOVA (F (6, 49) = 0.6610, $P = 0.6812$). A visible-platform test was also used to assess the visual condition and sensory-motor coordination of the subjects (Figs. 6H and I).

EXO Improves Aβ Clearance in the Hippocampus

To find Aβ plaques in the hippocampus of AD rats, Congo red staining was utilized. Amyloid plaques were found in the DG, CA1, and CA3 regions, and the STZ and STZ + EXO 0.7 groups had damaged granular and pyramidal cell layers. Compared to the control group, the hippocampus regions of STZ group showed a higher percentage of positive amyloid plaque areas. When compared to the STZ group, positively stained areas of amyloid plaques were significantly decreased in STZ + EXO7 and STZ + EXO70 (Fig. 7). The findings showed that EXO can decrease amyloid deposition in the hippocampus of AD rats.

EXO Increases the Presynaptic and Postsynaptic Markers Expression

We used Western blotting to show whether EXO has changed the level of proteins involved in neuronal plasticity, such as NMDAR1 and phosphorylated protein kinase Cα. In the homogenate of hippocampi, the antibodies particularly bind to their specific antigens. In the STZ group hippocampi, the level of p-PKC and NMDAR1 was significantly decreased, while in the STZ + EXO group, the levels of p-PKC (p 0.0017) and NMDAR1 (p 0.0198) were significantly increased (Fig. 8 and Figure S1). It means that treatment with EXO 70 enhances the expression and/or phosphorylation of p-PKC and the expression of NMDAR1 in the hippocampus and reversed the effects of STZ administration. Using immunofluorescence, we investigated the expression of GAP-43, synaptophysin, and integrin to show further effects of EXO on neuronal plasticity. In the brain sections, the antibodies particularly bind to their specific antigens. GAP-43 ($p = 0.0013$), synaptophysin ($p = 0.0004$), and integrin ($p = 0.0013$) showed statistically significant increases when compared to the STZ group's mean densitometric values (Fig. 8).

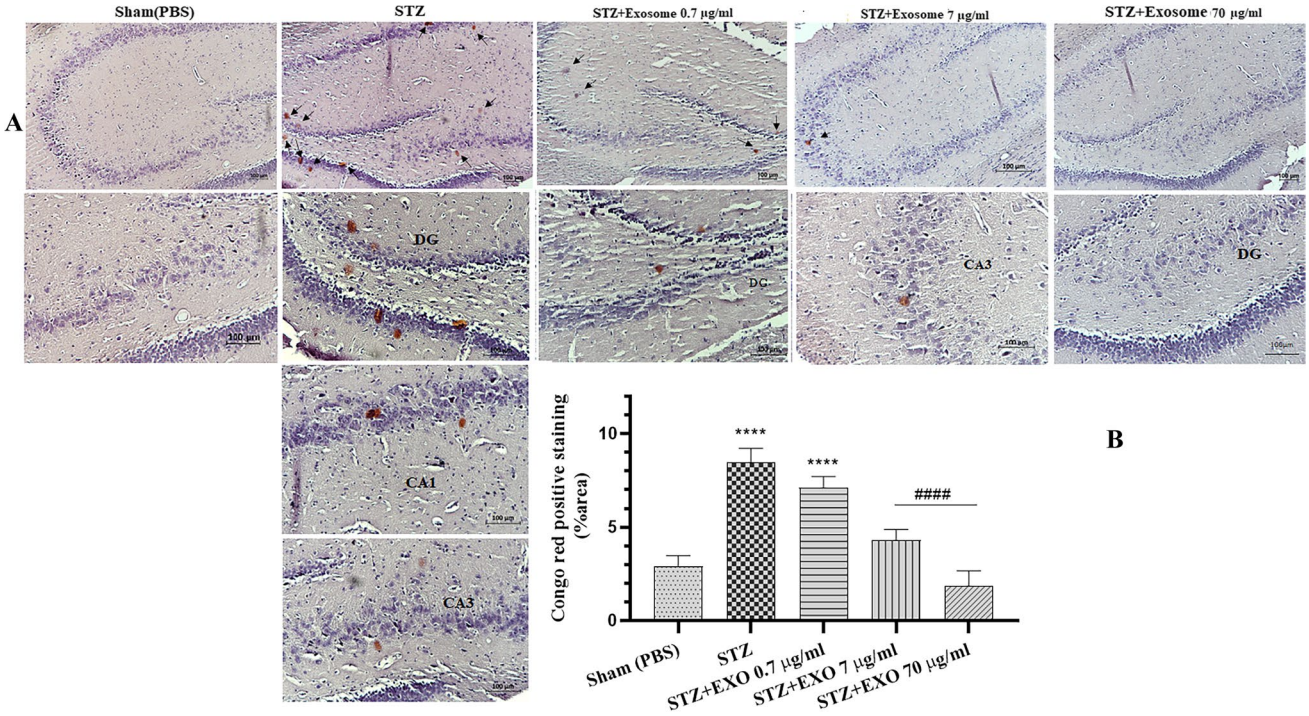

Fig. 7 **A** Congo Red staining in rat brain sections for amyloid plaque detection. Aβ deposition is stained in pink and is shown with a black arrow. Normal control showed an absence of amyloid deposition in the brain tissue. In the STZ group, amyloid deposition in the brain tissue was identified. Compared to the STZ group, administration of Exo 70 significantly reduced the number of amyloid plaques in brain tissue. **B** Quantitative assessment of the percentage area occupied by Aβ stain in hippocampal sections of rats' brains. The values are expressed as mean ± SD. $^{****}p < 0.0001$ compared to the sham group. $^{\#\#\#\#}p < 0.0001$ compared to the STZ group

The Effects of STZ and Exosomes on Neuroplasticity

STZ is a cytotoxic glucosamine-nitrosourea compound and is utilized to establish sporadic AD animal models [37]. STZ creates cross-links with fundamental structures and also induces free-radical generation [38]. Intracerebroventricular (ICV) injection of STZ in rats leads to disturbed insulin signaling pathways and glucose metabolism in the brain and also decreased cognitive abilities, the expression of neural plasticity markers, and neurotransmitters [39–41]. STZ induces oxidative condition, tau hyperphosphorylation, Aβ deposition, and neurotoxicity upon synaptic transmission (Fig. 9A) [39, 42–53]. Glutamate is the most abundant neurotransmitter in the nervous system and shows a fundamental role in learning and memory. The toxic amount of glutamate leads to neuronal cell death. Glutamate receptors, including NMDAR and AMPAR, bind to glutamate and have a significant role in synaptogenesis. Pyramidal neurons in the hippocampus are important neurons in learning and memory which can be activated with glutamate [54]. Growth associated protein 43 or GAP-43, is expressed at high levels in development, nerve growth, and axonal regeneration; thus, it is known as plasticity and growth protein in assessing the responses for nervous system regeneration. GAP-43 protein in rats can be phosphorylated by PKC on Ser41 site which plays an important role in guiding the nerve-terminal growth/axonal growth, stablishing new connections, and LTP (long-term potentiation). The phosphorylation of GAP-43 has a significant impact on its physiological activity. When Ca^{2+} levels are low, GAP-43 is bound by calmodulin, which prevents PKC from ser41 phosphorylation. This condition prevents GAP-43 from becoming activated in response to the second messenger. The calmodulin is dissociated as Ca^{2+} levels increase and PKC becomes active to phosphorylate the ser41 site [55–59]. By interacting with synaptophysin and SNAP, phosphorylated GAP-43 can control the recycling of vesicles in the synapse. In addition, it can regulate neurite outgrowth, endocytosis, and exocytosis [9]. Our results proved that EXOs can reverse the STZ effects on neuronal cells by changing the pre-and post-synaptic molecules expression (Fig. 9B).

Discussion

Learning and memory recovery can be considered major achievements in AD studies. We demonstrated that intranasal administrations of 3D-cultured hUSSCs derived EXO

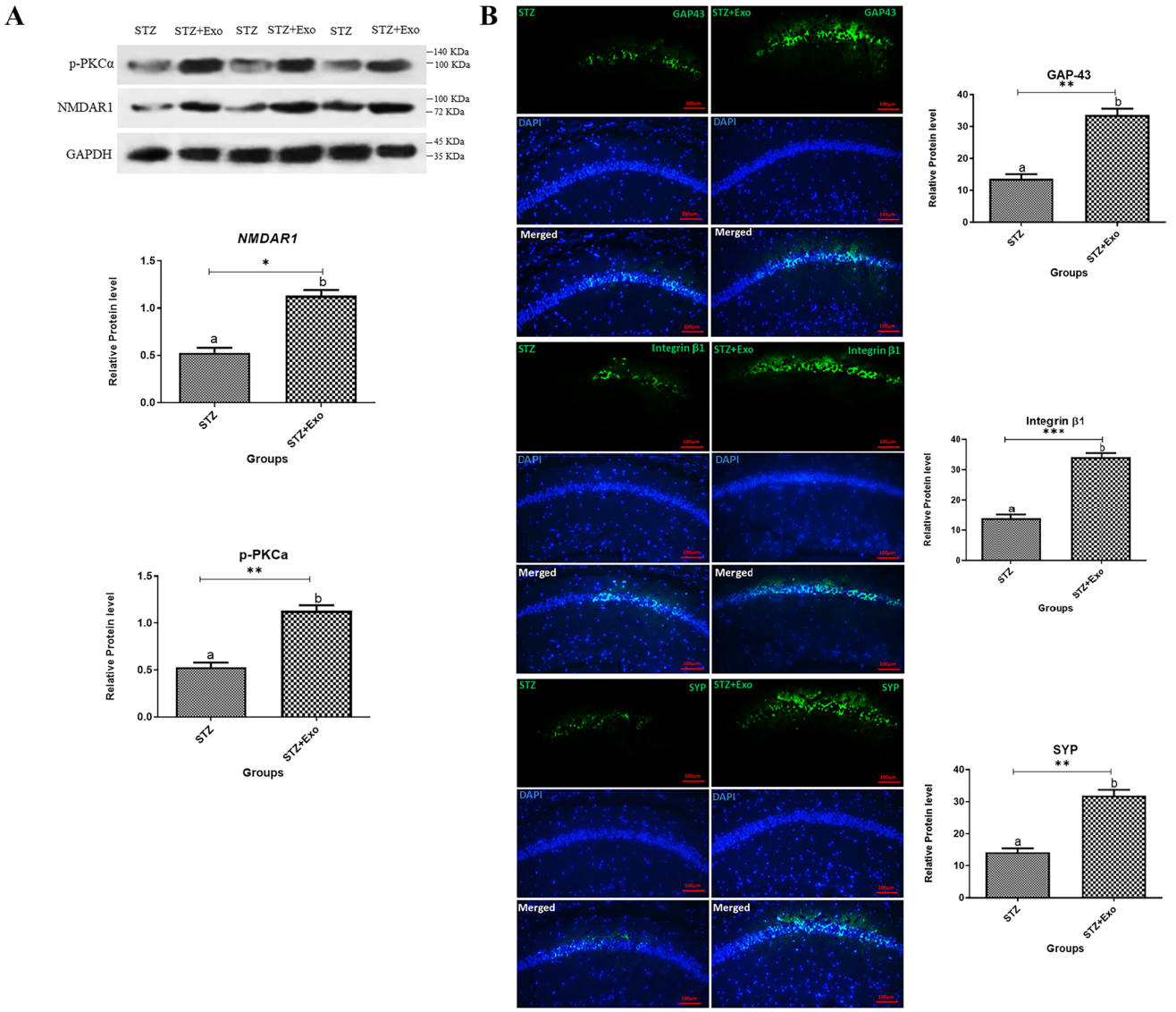

Fig. 8 **A** Western blot and quantification results of synaptic proteins and the housekeeping gene GAPDH in hippocampi from AD rats. Effects of administration of EXO on the expression of synapse-associated proteins in the rat hippocampus. Data are expressed as mean ± SEM, $n = 3$. $^{*}p < 0.0198$, $^{**}p < 0.0017$ versus the STZ group. **B** Brain tissues were fixed and stained with GAP-43, synaptophysin, and integrin antibodies and then imaged by immunofluorescence confocal microscopy (green). Nuclei were stained with DAPI (blue). The scale bar is 100 μm and applies to all figure parts. GAP-43 $p < 0.0013$**; Syn $p < 0.0004$***; integrin $p < 0.0013$*** in the CA1 region

improve memory and learning defects in the AD sporadic rat model after STZ injection in the brain. STZ injection is shown to increase Aβ accumulation in and out of cells and decrease neuronal presynaptic and postsynaptic genes' expression. The present study showed similar results [53, 60–64]. EXOs impressively play neuroprotective and immunomodulatory roles in the in vitro and in vivo studies; therefore, memory recovery likely suggests that the bioactive components of EXOs may negate the pathological mechanisms involved in memory loss. In many studies, the treatment with exosome has decreased Aβ deposition, pro-inflammatory factors secretion, and the apoptotic and necrotic cell populations, while it has increased viable cells percent and anti-inflammatory cytokines. Moreover, EXOs involve in neuroprotection, neurotransmission, neurogenesis, and axonal growth. In this way, our study results revealed that EXOs involve in neuro-regeneration procedures in rats [65–70].

hUSSCs, isolated from human umbilical cord blood, are a desirable population of stem cells that can be obtained at GMP grade without posing any ethical issues [71]. As evidence has increased, in comparison to conventional 2D

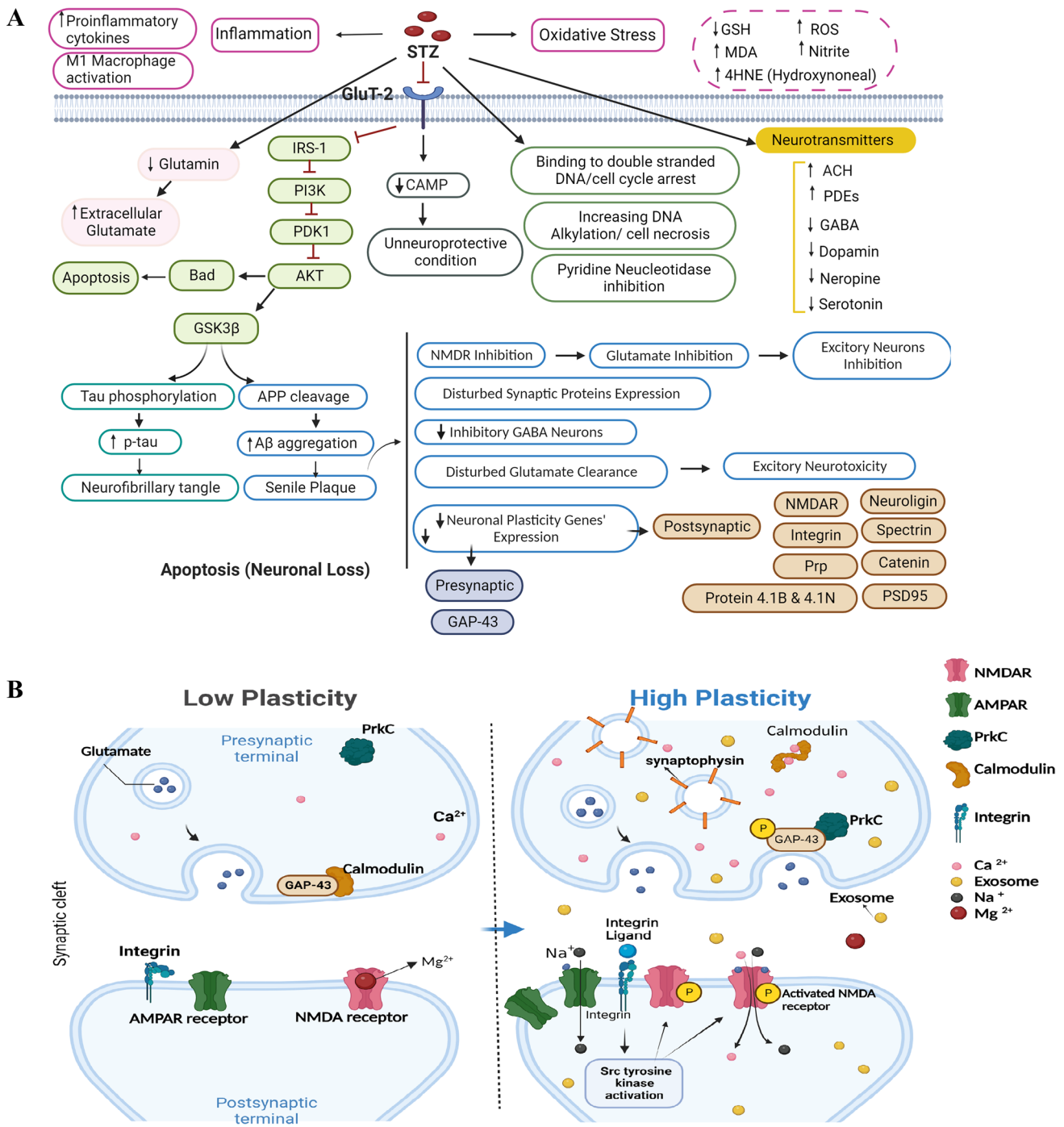

Fig. 9 **A** How STZ plays its destructive role in the brain. STZ declines cognitive abilities by creating cross-links with fundamental structures, inducing free-radical generation, disturbing insulin signaling pathways and glucose metabolism, decreasing neural plasticity markers, and neurotransmitter expression. It also induces oxidative conditions, tau hyperphosphorylation, Aβ deposition, and neurotoxicity upon synaptic transmission. Additionally, STZ leads to neuronal cell death by causing toxic levels of glutamate, impacting glutamate receptors, and phosphorylating GAP-43, which is important for nerve growth and regeneration. **B** The figure shows the pre-synaptic and post-synaptic molecules involved in high plasticity and their relationship. In low plasticity, calmodulin binds to GAP43 in pre-synapse, and NMDAR is inhibited by Mg^{2+}. In high plasticity, by increasing Ca^{2+} in neurons, PrkC starts the phosphorylation of GAP-43 and calmodulin binds to Ca^{2+}. NMADR is phosphorylated by Src tyrosine kinase (activated by integrin) and becomes activated. EXO was able to create a high plasticity condition. In high plasticity, the expression of molecules such as synaptophysin is increased. Figure created with BioRender.com

culture, 3D culture conditions appear to have a different effect on cells' behavior [29]. Through an increased number of cell-to-cell and cell-to-matrix interactions, 3D culture may provide a more realistic cellular physiology. For this aim, finding the initial number of cells for hUSSCs culture by the LOT technique was crucial, due to appropriate cell–cell interaction and nutrient availability [32]. In our study, we observed that if the number of cells is less than 5000/100 µl medium, the sizes of spheroids are small and their structure are fragile. At higher numbers, the spheroid size and structure are considerably changed. But, according to the volume of the medium, the maximum number of cells would be limited [32]. The protective effects of EXO were studied in the in vitro model of L-glutamate-induced cell damage, consisting of C6 cells cultured in 2D and 3D conditions and cells subjected to an apoptotic insult with L-glutamate. The in-vitro part of our study demonstrated that EXO derived from hUSSCs may play a neuroprotective role in the oxidative condition which is compatible with other studies in this field [65, 66, 72–74]. Compared to the glutamate group, hUSSCs-EXO increase the percent of live cells, as indicated by flow cytometry results and the fluorescent staining. The similar results have been described by other studies [70, 75, 76].

As generally reported, ICV injection of STZ in rats could provide a reliable model of AD, and the STZ dose selection in this study was consistent with the dose selection in other studies [35, 60]. We used STZ because Ting Ju and colleagues have proved that STZ injures the structure of synapses and synaptic transmission in rats' pyramidal neurons in the CA1 region [53]. According to the findings, STZ inhibits synaptic transmission, likely leading to cytotoxicity and cognitive impairments. In the early stages of AD, defects in synaptic transmission have been detected, showing that the rat induced by STZ can be an effective model to study the mechanisms involved in neuronal growth and degeneration during AD [77, 78]. As a result, providing a healthy synaptic transmission may be considered a novel and significant treatment option for AD. Our findings confirmed that the STZ injection leads to learning and memory-damaging conditions [36, 79, 80].

STZ had no effect on visible platform tasks in the MWM test, indicating that the observed impairment was unrelated to its effect on the motivation of animals or their visual-motor ability. The STZ group treated with EXO showed decreased latency to the first cross of the platform's place and more crossing frequency. These groups also spent much more time on the location of the platform; thus, applying EXOs in the rat can reduce the negative effects of STZ. The different doses of EXOs showed dose-dependent results that suggested 70 µg/ml has more effective results in the MWM test in comparison with 7 and 0.7.

The benefits of administering MSC-derived EXOs as a promising tool for cell-free therapy in AD rats, previous reports, were confirmed by our findings [70, 75, 81–84]. The studies have proved the effects of EXOs on reducing β-amyloid pathology and neuronal regeneration, which improved cognition impairment [70, 75, 76]. Exosomes' effects on neuronal plasticity have been the subject of a few studies [85]. Increasing the NMDAR in the CA1 region in the hippocampus shows that the neurons are more involved in learning and memory procedures after EXO treatment in comparison to the STZ group, which shows a low expression level in the same region. Synaptic plasticity, synaptogenesis, learning, and memory all depend on the protein NMDAR. In fact, in NMDAR proper activity, integrins (α3β1, α5β1, α8β1) has the crucial role. Integrins are involved in synaptic transmission, synaptic plasticity, and also LTP. It has been proven that integrins involve in the process to prevent the LTP inhibiting induced by Aβ, and in our study, integrin showed increased expression after EXO treatment [54]. High levels of integrins (adhesion proteins affecting the function of nearby transmembrane proteins) have been detected at synapses. Studies have shown that integrins have a significant role in LTP consolidation by tyrosine kinase activation (such as Src) and NMDAR regulation. Since Src activation can phosphorylate the subunit of the NMDAR, it can increase the currents of the receptor and induce LTP (Fig. 9B) [86]. Similar to Lin's study, our findings demonstrate that treatment with EXO increases NMDAR and integrin receptor expression in the hippocampus [87]. The results show that hUSSCs- EXOs mediate direct neuro-regeneration by increasing the pPKC and GAP-43 levels in the neuronal cell, which was similar to Hao's study [88]. It has been demonstrated in several investigations that STZ therapy reduces GAP-43 and SYN levels; herein, we reveal that, in comparison to the STZ group, EXO-treated rats have increased levels of GAP-43 and SYN expression in the hippocampus. The effect of EXO on cognitive deficit improvement could result from its potential to increase GAP-43 and SYN protein levels in the STZ-induced hippocampus. The declining level of functional proteins in the synapse leads to its dysfunctionality. For example, in plasma neuronal-derived exosomes (NDEs), the levels of synaptophysin and GAP-43 were significantly decreased in AD patients [89].

These results are similar to other studies, showing that MSC-EXO treatment improved learning and memory capacities, decreased the Aβ deposition, and increased the expression level of GAP-43, synapsin 1, and IL-10 [90–93]. In AD, there is an imbalance between biosynthesis and the elimination of Aβ that plays a neurotoxic role in the synapses and changes communication.

and therefore decreases the learning and memory capabilities [94]. Congo red staining in our study confirmed the amyloid deposition in the STZ rat hippocampus and also showed that EXO can decrease Aβ deposition in the hippocampus, as other studies have mentioned [66, 75]. In

EXO-treated groups, learning and memory abilities were improved, which can be linked to Aβ removal as was seen in Congo red staining [95]. Intranasal administration is a method with desirable attributes such as minimum invasiveness, repeatability, simplicity of operation, and a semi-direct transporting route. The treatment cargo is transported across a single layer of epithelial cells to blood circulation or through the olfactory nerve cells and blood–brain barrier into the brain (Fig. 1) [68, 96].

In this study, the MWM test revealed impairments in spatial learning and memory capabilities in STZ-induced rats. We proved that regular administration of EXO at high dose for 2 weeks dramatically reversed behavioral abnormalities and cognitive deficits in rats. The effects of EXO are related to increasing the expression of neuronal plasticity target genes in presynapse and postsynapse that are decreased by STZ injection. In addition, the newly produced synaptic proteins and synaptic RNAs would then be transferred by the EXOs to the presynaptic terminal and participate in synaptic plasticity[97].

Conclusion

The 3D-cultured-hUSSCs derived EXO protect cells in cytotoxic circumstances, and improve memory and learning deficits in the rat model of Alzheimer's disease. hUSSCs-derived EXOs intranasal administration in sporadic AD rats fully restores rat memory and impressively changes neuronal synapse state. The protective role of EXO may be related to the increased level of GAP-43, synaptophysin, NMDAR1, integrin, and pPKC in the hippocampus which can improve spatial learning and memory deficits in AD rats.

Abbreviations AD: Alzheimer's disease; Aβ: Beta-amyloid; NMDA: N-methyl-d-aspartate; GAP-43: Growth-associated protein; PKC: Protein kinase C; USSCs: Unrestricted somatic stem cells; LOT: Liquid overlay technique; STZ: Streptozotocin; EXO: Exosomes; NH4Cl: Ammonium chloride; HBSS: Hank's balanced salt solution; FBS: Fetal bovine serum; IBMX: Isobutyl-methylxanthine; ICV: Intracerebroventricular; LTP: Long-term potentiation

Supplementary Information The online version contains supplementary material available at https://doi.org/10.1007/s12035-023-03733-w.

Acknowledgements We acknowledge and thank the Medical Nanotechnology and Tissue Engineering Research Center for the financial support.

Author Contribution This article is extracted from the Ph.D. thesis by M.P. at Shahid Beheshti University of Medical Sciences, Tehran, Iran. H.Z. designed and supervised the in vitro section, and R.Gh. supervised the in vivo section of the study. M.P. designed and carried out all laboratory jobs—in vitro and in vivo sections—data collection and analysis, figures preparation, manuscript writing, and manuscript revision. M.S. helped with stem cell extraction, and F.M. and M.F. consulted in the in vivo study design. The authors read and approved the final manuscript.

Funding This work was supported by the Medical Nanotechnology and Tissue Engineering Research Center, Shahid Beheshti University of Medical Sciences, Tehran, Iran (Grant/Award Number: 31169).

Data Availability The datasets used and/or analyzed during the current study are available from the corresponding authors on reasonable request.

Declarations

Ethics Approval and Consent to Participate The study was approved by the Medical Ethics Committee of Shahid Beheshti University of Medical Sciences and Gandi Hospital (IR.SBMU.AEC.1401.005). Written informed consent was obtained from mothers in the hospital.

Consent for Publication Not applicable.

Competing Interests The authors declare no competing interests.

References

1. Williams A (2002) Defining neurodegenerative diseases: disorders will be named after responsible rogue proteins and their solutions. British Medical Journal Publishing Group, pp 1465–1466
2. Khanahmadi M, Farhud DD, Malmir M (2015) Genetic of Alzheimer's disease: a narrative review article. Iran J Public Health 44(7):892
3. Mattson MP et al (1999) Cellular and molecular mechanisms underlying perturbed energy metabolism and neuronal degeneration in Alzheimer's and Parkinson's diseases. Ann N Y Acad Sci 893(1):154–175
4. Tampellini D (2015) Synaptic activity and Alzheimer's disease: a critical update. Front Neurosci 9:423
5. Tampellini D et al (2010) Effects of synaptic modulation on β-amyloid, synaptophysin, and memory performance in Alzheimer's disease transgenic mice. J Neurosci 30(43):14299–14304
6. Crupi R, Impellizzeri D, Cuzzocrea S (2019) Role of metabotropic glutamate receptors in neurological disorders. Front Mol Neurosci 12:20
7. Malinow R (2012) New developments on the role of NMDA receptors in Alzheimer's disease. Curr Opin Neurobiol 22(3):559–563
8. Wennström M, Nielsen HM (2012) Cell adhesion molecules in Alzheimer's disease. Degener Neurol Neuromuscul Dis 2:65
9. Grabczyk E et al (1990) Cloning and characterization of the rat gene encoding GAP-43. Eur J Neurosci 2(10):822–827
10. Holahan MR (2015) GAP-43 in synaptic plasticity: molecular perspectives. Res Rep Biochem 5:137–146
11. Snipes G et al (1987) Evidence for the coidentification of GAP-43, a growth-associated protein, and F1, a plasticity-associated protein. J Neurosci 7(12):4066–4075
12. Holahan MR (2017) A shift from a pivotal to supporting role for the growth-associated protein (GAP-43) in the coordination of axonal structural and functional plasticity. Front Cell Neurosci 11:266
13. Florez JC, Nelson RB, Routtenberg A (1991) Contrasting patterns of protein phosphorylation in human normal and Alzheimer brain: focus on protein kinase C and protein F1GAP-43. Exp Neurol 112(3):264–272
14. Yan Y et al (2014) Adipose-derived mesenchymal stem cell transplantation promotes adult neurogenesis in the brains of Alzheimer's disease mice. Neural Regen Res 9(8):798

15. Park B-N et al (2020) Therapeutic effect of mesenchymal stem cells in an animal model of Alzheimer's disease evaluated by β-amyloid positron emission tomography imaging. Aust N Z J Psychiatry 54(9):883–891
16. Kanamaru T et al (2015) Intravenous transplantation of bone marrow-derived mononuclear cells prevents memory impairment in transgenic mouse models of Alzheimer's disease. Brain Res 1605:49–58
17. Wu Q-Y et al (2007) Bone marrow stromal cells of transgenic mice can improve the cognitive ability of an Alzheimer's disease rat model. Neurosci Lett 417(3):281–285
18. Zhang X-M et al (2021) Therapeutic potential of dental pulp stem cell transplantation in a rat model of Alzheimer's disease. Neural Regen Res 16(5):893
19. Kim DY et al (2020) Feasibility and efficacy of intra-arterial administration of embryonic stem cell derived-mesenchymal stem cells in animal model of Alzheimer's disease. J Alzheimers Dis 76(4):1281–1296
20. Lee HJ et al (2012) Human umbilical cord blood-derived mesenchymal stem cells improve neuropathology and cognitive impairment in an Alzheimer's disease mouse model through modulation of neuroinflammation. Neurobiol Aging 33(3):588–602
21. Kim KY, Suh Y-H, Chang K-A (2020) Therapeutic effects of human amniotic epithelial stem cells in a transgenic mouse model of Alzheimer's disease. Int J Mol Sci 21(7):2658
22. Oh SH et al (2015) Mesenchymal stem cells increase hippocampal neurogenesis and neuronal differentiation by enhancing the Wnt signaling pathway in an Alzheimer's disease model. Cell Transplant 24(6):1097–1109
23. Yun H et al (2013) Placenta-derived mesenchymal stem cells improve memory dysfunction in an Aβ1–42-infused mouse model of Alzheimer's disease. Cell Death Dis 4(12):e958–e958
24. Esmaeilzade B et al (2019) Dimethyloxalylglycine preconditioning enhances protective effects of bone marrow-derived mesenchymal stem cells in Aβ-induced Alzheimer disease. Physiol Behav 199:265–272
25. Nasiri E et al (2019) Melatonin-pretreated adipose-derived mesenchymal stem cells efficiently improved learning, memory, and cognition in an animal model of Alzheimer's disease. Metab Brain Dis 34(4):1131–1143
26 Pourhadi M et al (2022) Promising role of oral cavity mesenchymal stem cell-derived extracellular vesicles in neurodegenerative diseases. Mol Neurobiol 59(10):6125–6140
27. Schira J et al (2015) Characterization of regenerative phenotype of unrestricted somatic stem cells (USSC) from human umbilical cord blood (hUCB) by functional secretome analysis. Mol Cell Proteomics 14(10):2630–2643
28. Broxmeyer HE et al (2011) Hematopoietic stem/progenitor cells, generation of induced pluripotent stem cells, and isolation of endothelial progenitors from 21-to 23.5-year cryopreserved cord blood. Blood, J Am Soc Hematol 117(18):4773–4777
29. Haraszti RA et al (2018) Exosomes produced from 3D cultures of MSCs by tangential flow filtration show higher yield and improved activity. Mol Ther 26(12):2838–2847
30. Tsai A-C et al (2015) Compaction, fusion, and functional activation of three-dimensional human mesenchymal stem cell aggregate. Tissue Eng Part A 21(9–10):1705–1719
31. Costa EC et al (2018) Spheroids formation on non-adhesive surfaces by liquid overlay technique: considerations and practical approaches. Biotechnol J 13(1):1700417
32. Costa EC et al (2014) Optimization of liquid overlay technique to formulate heterogenic 3D co-cultures models. Biotechnol Bioeng 111(8):1672–1685
33. Cheng N-C et al (2013) Short-term spheroid formation enhances the regenerative capacity of adipose-derived stem cells by promoting stemness, angiogenesis, and chemotaxis. Stem Cells Transl Med 2(8):584–594
34 Pourhadi M et al (2022) Cuscuta epithymum Murr. crude extract pre-conditioning protects C6 cells from L-glutamate-induced neurotoxicity. BMC Complement Med Ther 22(1):335
35. Javadpour P et al (2021) Imipramine alleviates memory impairment and hippocampal apoptosis in STZ-induced sporadic Alzheimer's rat model: possible contribution of MAPKs and insulin signaling. Behav Brain Res 408:113260
36. Moosavi M et al (2020) Effect of carbamylated erythropoietin Fc fusion protein (CEPO-Fc) on learning and memory impairment and hippocampal apoptosis induced by intracerebroventricular administration of streptozotocin in rats. Behav Brain Res 384:112554
37. Bolzán AD, Bianchi MS (2002) Genotoxicity of streptozotocin. Mutat Res/Rev Mutat Res 512(2–3):121–134
38. Eleazu CO et al (2013) Review of the mechanism of cell death resulting from streptozotocin challenge in experimental animals, its practical use and potential risk to humans. J Diabetes Metab Disord 12(1):1–7
39. Grünblatt E et al (2007) Brain insulin system dysfunction in streptozotocin intracerebroventricularly treated rats generates hyperphosphorylated tau protein. J Neurochem 101(3):757–770
40. Chen Y et al (2013) A non-transgenic mouse model (icv-STZ mouse) of Alzheimer's disease: similarities to and differences from the transgenic model (3xTg-AD mouse). Mol Neurobiol 47(2):711–725
41. Deng PY, Lei S (2006) Bidirectional modulation of GABAergic transmission by cholecystokinin in hippocampal dentate gyrus granule cells of juvenile rats. J Physiol 572(2):425–442
42. Sharma M, Gupta Y (2001) Intracerebroventricular injection of streptozotocin in rats produces both oxidative stress in the brain and cognitive impairment. Life Sci 68(9):1021–1029
43. Salkovic-Petrisic M et al (2011) Cerebral amyloid angiopathy in streptozotocin rat model of sporadic Alzheimer's disease: a long-term follow up study. J Neural Transm 118(5):765–772
44. Ishrat T et al (2009) Selenium prevents cognitive decline and oxidative damage in rat model of streptozotocin-induced experimental dementia of Alzheimer's type. Brain Res 1281:117–127
45. Salkovic-Petrisic M et al (2014) Long-term oral galactose treatment prevents cognitive deficits in male Wistar rats treated intracerebroventricularly with streptozotocin. Neuropharmacology 77:68–80
46. Zhou S et al (2013) Neuroprotective effects of edaravone on cognitive deficit, oxidative stress and tau hyperphosphorylation induced by intracerebroventricular streptozotocin in rats. Neurotoxicology 38:136–145
47. Gutierres JM et al (2014) Anthocyanins restore behavioral and biochemical changes caused by streptozotocin-induced sporadic dementia of Alzheimer's type. Life Sci 96(1–2):7–17
48. Nayebi AM, Pourrabi S, Hossini S (2014) Testosterone ameliorates streptozotocin-induced memory impairment in male rats. Acta Pharmacol Sin 35(6):752–757
49. Xu Z-P et al (2014) Magnesium protects cognitive functions and synaptic plasticity in streptozotocin-induced sporadic Alzheimer's model. PLoS ONE 9(9):e108645
50. Zamani M et al (2015) Pre-training Catechin gavage prevents memory impairment induced by intracerebroventricular streptozotocin in rats. Neurosci J 20(3):225–229
51. Wang H et al (2016) Ameliorating effect of luteolin on memory impairment in an Alzheimer's disease model. Mol Med Rep 13(5):4215–4220
52. Peng D et al (2013) Hyperphosphorylation of tau protein in hippocampus of central insulin-resistant rats is associated with cognitive impairment. Cell Physiol Biochem 32(5):1417–1425
53. Ju T et al (2016) Streptozotocin inhibits electrophysiological determinants of excitatory and inhibitory synaptic transmission in CA1 pyramidal neurons of rat hippocampal slices:

reduction of these effects by edaravone. Cell Physiol Biochem 40(6):1274–1288
54. Rowan M et al (2007) Synaptic memory mechanisms: Alzheimer's disease amyloid β-peptide-induced dysfunction. Biochem Soc Trans 35(5):1219–1223
55. Sheu F-S et al (1990) Neuron-specific protein F1GAP-43 shows substrate specificity for the beta subtype of protein kinase C. Biochem Biophys Res Commun 171(3):1236–1243
56. Rosenthal A et al (1987) Primary structure and mRNA localization of protein F1, a growth-related protein kinase C substrate associated with synaptic plasticity. EMBO J 6(12):3641–3646
57. Chao S et al (1996) Use of a two-hybrid system to investigate molecular interactions of GAP-43. Mol Brain Res 40(2):195–202
58. Kumar V et al (2013) Structural basis for the interaction of unstructured neuron specific substrates neuromodulin and neurogranin with Calmodulin. Sci Rep 3(1):1–9
59. Neve RL et al (1998) The neuronal growth-associated protein GAP-43 interacts with rabaptin-5 and participates in endocytosis. J Neurosci 18(19):7757–7767
60. Ju T et al (2016) Streptozotocin inhibits synaptic transmission and edaravone attenuates streptozotocin-induced electrophysiological changes in CA1 pyramidal neurons of rat hippocampal slices. Neurotoxicology 57:75–86
61. Kamal A et al (2006) Synaptic transmission changes in the pyramidal cells of the hippocampus in streptozotocin-induced diabetes mellitus in rats. Brain Res 1073:276–280
62. Qi C-C et al (2021) Impaired learning and memory ability induced by a bilaterally hippocampal injection of streptozotocin in mice: involved with the adaptive changes of synaptic plasticity. Front Aging Neurosci 13:633495
63. Zhao F et al (2016) Changes in neurons and synapses in hippocampus of streptozotocin-induced type 1 diabetes rats: a stereological investigation. Anat Rec 299(9):1174–1183
64. Park J et al (2020) Streptozotocin Induces Alzheimer's disease-like pathology in hippocampal neuronal cells via CDK5/Drp1-mediated mitochondrial fragmentation. Front Cell Neurosci 14:235
65. Ahmed NE-MB et al (2016) Therapeutic potential of dental pulp stem cell secretome for Alzheimer's disease treatment: an in vitro study. Stem Cells Int 2016:11
66. Lee M et al (2018) The exosome of adipose-derived stem cells reduces β-amyloid pathology and apoptosis of neuronal cells derived from the transgenic mouse model of Alzheimer's disease. Brain Res 1691:87–93
67. Losurdo M et al (2020) Intranasal delivery of mesenchymal stem cell-derived extracellular vesicles exerts immunomodulatory and neuroprotective effects in a 3xTg model of Alzheimer's disease. Stem Cells Transl Med 9(9):1068–1084
68. Mita T et al (2015) Conditioned medium from the stem cells of human dental pulp improves cognitive function in a mouse model of Alzheimer's disease. Behav Brain Res 293:189–197
69. Elia CA et al (2019) Intracerebral injection of extracellular vesicles from mesenchymal stem cells exerts reduced Aβ plaque burden in early stages of a preclinical model of Alzheimer's disease. Cells 8(9):1059
70. Reza-Zaldivar EE et al (2019) Mesenchymal stem cell-derived exosomes promote neurogenesis and cognitive function recovery in a mouse model of Alzheimer's disease. Neural Regen Res 14(9):1626
71. Schira J et al (2015) Characterization of regenerative phenotype of unrestricted somatic stem cells from human umbilical cord blood by functional secretome analysis. Mol Cell Proteomics 14(10):2630–2643
72. Bonafede R et al (2019) The anti-apoptotic effect of ASC-exosomes in an in vitro ALS model and their proteomic analysis. Cells 8(9):1087
73. Venugopal C et al (2017) Dosage and passage dependent neuroprotective effects of exosomes derived from rat bone marrow mesenchymal stem cells: an in vitro analysis. Curr Gene Ther 17(5):379–390
74. Thomi G et al (2019) Intranasally administered exosomes from umbilical cord stem cells have preventive neuroprotective effects and contribute to functional recovery after perinatal brain injury. Cells 8(8):855
75. Yang L et al (2020) The regulatory functionality of exosomes derived from hUMSCs in 3D culture for Alzheimer's disease therapy. Small 16(3):1906273
76. Zhdanova DY et al (2021) Effect of intranasal administration of multipotent mesenchymal stromal cell exosomes on memory of mice in Alzheimer's disease model. Bull Exp Biol Med 170(4):575–582
77. Selkoe DJ (2002) Alzheimer's disease is a synaptic failure. Science 298(5594):789–791
78. Parameshwaran K, Dhanasekaran M, Suppiramaniam V (2008) Amyloid beta peptides and glutamatergic synaptic dysregulation. Exp Neurol 210(1):7–13
79. Tota S et al (2011) Improvement of brain energy metabolism and cholinergic functions contributes to the beneficial effects of silibinin against streptozotocin induced memory impairment. Behav Brain Res 221(1):207–215
80. Rai S et al (2014) Glial activation and post-synaptic neurotoxicity: the key events in Streptozotocin (ICV) induced memory impairment in rats. Pharmacol Biochem Behav 117:104–117
81. Nakano M et al (2016) Bone marrow-derived mesenchymal stem cells improve diabetes-induced cognitive impairment by exosome transfer into damaged neurons and astrocytes. Sci Rep 6(1):1–14
82. Zhang Y et al (2017) Systemic administration of cell-free exosomes generated by human bone marrow derived mesenchymal stem cells cultured under 2D and 3D conditions improves functional recovery in rats after traumatic brain injury. Neurochem Int 111:69–81
83. Ding M et al (2018) Exosomes isolated from human umbilical cord mesenchymal stem cells alleviate neuroinflammation and reduce amyloid-beta deposition by modulating microglial activation in Alzheimer's disease. Neurochem Res 43(11):2165–2177
84. Nakano M et al (2020) Bone marrow-derived mesenchymal stem cells improve cognitive impairment in an Alzheimer's disease model by increasing the expression of microRNA-146a in hippocampus. Sci Rep 10(1):1–15
85. An K et al (2013) Exosomes neutralize synaptic-plasticity-disrupting activity of Aβ assemblies in vivo. Mol Brain 6(1):1–13
86. Lu YM et al (1998) Src activation in the induction of long-term potentiation in CA1 hippocampal neurons. Science 279(5355):1363–1368
87. Lin B et al (2003) Integrins regulate NMDA receptor-mediated synaptic currents. J Neurophysiol 89(5):2874–2878
88. Hao P et al (2014) Conditioned medium of human adipose-derived mesenchymal stem cells mediates protection in neurons following glutamate excitotoxicity by regulating energy metabolism and GAP-43 expression. Metab Brain Dis 29(1):193–205
89. Goetzl EJ et al (2016) Decreased synaptic proteins in neuronal exosomes of frontotemporal dementia and Alzheimer's disease. FASEB J 30(12):4141–4148
90. Cui GH et al (2018) Exosomes derived from hypoxia-preconditioned mesenchymal stromal cells ameliorate cognitive decline by rescuing synaptic dysfunction and regulating inflammatory responses in APP/PS1 mice. FASEB J 32(2):654–668
91. Ma Y et al (2017) Mesenchymal stem cell-derived extracellular vesicles promote nerve regeneration after sciatic nerve crush injury in rats. Int J Clin Exp Pathol 10(9):10032
92. Di-fan Z et al (2021) Bone marrow mesenchymal stem cell-derived exosomes treat sciatic nerve injury recovery by promoting axonal regeneration. Lingnan Modern Clin Surg 21(02):182

93. Cizkova D et al (2018) Localized intrathecal delivery of mesenchymal stromal cells conditioned medium improves functional recovery in a rat model of spinal cord injury. Int J Mol Sci 19(3):870
94. Tai C-Y, Kim SA, Schuman EM (2008) Cadherins and synaptic plasticity. Curr Opin Cell Biol 20(5):567–575
95. Mehrabadi S et al (2020) Hypoxic-conditioned medium from adipose tissue mesenchymal stem cells improved neuroinflammation through alternation of toll like receptor (TLR) 2 and TLR4 expression in model of Alzheimer's disease rats. Behav Brain Res 379:112362
96. Haney MJ et al (2015) Exosomes as drug delivery vehicles for Parkinson's disease therapy. J Control Release 207:18–30
97. Smalheiser NR (2007) Exosomal transfer of proteins and RNAs at synapses in the nervous system. Biol Direct 2(1):1–15